HAL
open science

An axisymmetric evolution code for the Einstein equations on hyperboloidal slices

Oliver Rinne

To cite this version:

Oliver Rinne. An axisymmetric evolution code for the Einstein equations on hyperboloidal slices. Classical and Quantum Gravity, 2010, 27 (3), pp.35014. 10.1088/0264-9381/27/3/035014 . hal-00569776

HAL Id: hal-00569776

https://hal.science/hal-00569776v1

Submitted on 25 Feb 2011

HAL is a multi-disciplinary open access archive for the deposit and dissemination of scientific research documents, whether they are published or not. The documents may come from teaching and research institutions in France or abroad, or from public or private research centers.

L'archive ouverte pluridisciplinaire **HAL**, est destinée au dépôt et à la diffusion de documents scientifiques de niveau recherche, publiés ou non, émanant des établissements d'enseignement et de recherche français ou étrangers, des laboratoires publics ou privés.

Confidential: not for distribution. Submitted to IOP Publishing for peer review 8 December 2009

An axisymmetric evolution code for the Einstein equations on hyperboloidal slices

Oliver Rinne

Department of Applied Mathematics and Theoretical Physics, Centre for Mathematical Sciences, Wilberforce Road, Cambridge CB3 0WA, UK
and
King's College, Cambridge CB2 1ST, UK

E-mail: O.Rinne@damtp.cam.ac.uk

Abstract. We present the first stable dynamical numerical evolutions of the Einstein equations in terms of a conformally rescaled metric on hyperboloidal hypersurfaces extending to future null infinity. Axisymmetry is imposed in order to reduce the computational cost. The formulation is based on an earlier axisymmetric evolution scheme, adapted to time slices of constant mean curvature. Ideas from a previous study by Moncrief and the author are applied in order to regularize the formally singular evolution equations at future null infinity. Long-term stable and convergent evolutions of Schwarzschild spacetime are obtained, including a gravitational perturbation. The Bondi news function is evaluated at future null infinity.

PACS numbers: 04.20.Cv, 04.20.Ha, 04.25.D-, 04.30.-w

1. Introduction

A major problem in numerical relativity that is currently attracting considerable interest is the global treatment of entire asymptotically flat spacetimes. This is relevant both to the modelling of the gravitational radiation emitted by compact astrophysical sources, and to several questions in mathematical relativity such as the nonlinear stability of black holes and the quantitative asymptotic behaviour of perturbations of such spacetimes.

In the standard approach based on the Cauchy formulation, one truncates the spatial domain at a finite distance from the source, where boundary conditions must be supplied (see [1] for a review). Apart from being compatible with the Einstein constraint equations and yielding a well-posed initial-boundary value problem, these boundary conditions must carefully take into account the propagation of gravitational radiation. For instance, crude choices of boundary conditions are known to lead to incorrect results on radiation tails in the evolution of perturbed black hole spacetimes [2, 3]. Recently, improved absorbing boundary conditions that minimize spurious reflections of gravitational radiation have been derived and implemented [4, 5, 6]. While constituting a significant improvement, this approach still relies on the assumption that the Einstein equations may be linearized about a given background spacetime so that incoming and outgoing radiation can be identified—an assumption that may not always be valid [7]. In the full nonlinear theory there is no satisfactory

quasi-local definition of a gravitational energy flux at a finite distance from the source [8]. This fact also complicates the extraction of gravitational radiation in an invariant manner.

Gravitational radiation is only unambiguously defined at future null infinity $\mathscr{I}^+$ [9, 10]. Thus it is very desirable to include $\mathscr{I}^+$ in the computational domain. There are several ways of doing this. One approach is characteristic evolution, whereby spacetime is foliated by null hypersurfaces that can be compactified towards $\mathscr{I}^+$ (see [11] for a review). This works well in the far field but characteristic foliations are ill behaved in strong-field regions due to the formation of caustics in the null congruences generating the hypersurfaces. A compromise is Cauchy-characteristic matching, where a Cauchy evolution in the interior is matched to a characteristic evolution in an exterior region. In [12] this has recently been applied to the *a posteriori* extraction of gravitational radiation from a Cauchy evolution (with finite outer boundary) of a binary black hole coalescence.

A more efficient solution is a foliation of spacetime into hyperboloidal hypersurfaces, which are everywhere spacelike but approach future null infinity rather than spacelike infinity. Such surfaces are not Cauchy surfaces—the foliation covers only the region to the future of some initial hyperboloidal hypersurface but not, for instance, the region around spacelike infinity. This is not a serious disadvantage for the applications we have in mind as we are mainly interested in computing the gravitational radiation at $\mathscr{I}^+$ and studying the late-time behaviour of perturbations. Hyperboloidal foliations have the advantage of being as flexible as standard Cauchy foliations in the interior, so that a variety of gauge conditions can be used that have been known to be successful in strong-field situations. In [13] Friedrich reformulated the Einstein equations for a conformally rescaled metric in such a way that they are manifestly regular at $\mathscr{I}^+$. This symmetric hyperbolic system is larger than the actual Einstein equations, e.g. it contains evolution equations for the Weyl curvature. For reviews of the theoretical development as well as numerical implementations, we refer the reader to [14, 15, 16]. Perhaps most relevant to the present work is an axisymmetric reduction of the regular conformal field equations by Frauendiener and Hein [17] that was applied to the numerical evolution of Minkowski spacetime and the boost-axisymmetric solutions of Bičák and Schmidt [18].

Despite these successes, most recent work in numerical relativity has used formulations of the Einstein equations (usually on truncated Cauchy hypersurfaces) rather than the regular conformal field equations. For this reason, it is worth investigating whether some formulation of the Einstein equations themselves can be adapted to hyperboloidal foliations reaching out to $\mathscr{I}^+$. As for the regular conformal field equations, one applies a conformal transformation to the metric in order to map $\mathscr{I}^+$ to a finite coordinate location in a compactified coordinate system, where the conformal factor vanishes. When written in terms of the conformal metric, the Einstein equations contain inverse powers of the conformal factor, terms that are singular at $\mathscr{I}^+$. Numerical implementations must face the question of how to deal with these formally singular terms, which may be potential sources of instabilities.

One proposal for solving the Einstein equations on hyperboloidal slices was developed by Zenginoğlu [19]. It combines a conformal transformation of the spacetime metric (where the conformal factor can essentially be freely specified) with a certain choice of gauge source functions for the Einstein equations in (generalized) harmonic gauge [20]. Preliminary numerical results on spherically symmetric evolutions of Schwarzschild spacetime were reported in section 2.5 of [21]. However, it is not yet

clear how the formally singular terms at $\mathscr{I}^+$ are to be evaluated numerically in more general situations.

Here we follow a different approach due to Moncrief that is based on an ADM-like [22] formulation of the Einstein equations with a constant-mean-curvature (CMC) slicing condition. In [23] we showed explicitly how the formally singular terms in the evolution equations at $\mathscr{I}^+$ can be evaluated there in terms of conformally regular geometric data. The constraint equations that occur in this approach were solved numerically in [24] and initial data on CMC slices describing various configurations of single and binary black holes were constructed. The present paper is concerned with the evolution problem. We assume spacetime to be axisymmetric in order to speed up the code so that different ways of treating $\mathscr{I}^+$ numerically can be experimented with. We apply the ideas of [23] to an earlier axisymmetric evolution scheme on Cauchy slices [25] (see also [26, 27] for related schemes). The objective of the paper is to show that long-term stable evolutions are possible, including gravitational radiation.

The paper is organized as follows. In section 2 we explain our notation and gauge choices and obtain the constraint and evolution equations. Particular emphasis is placed on how the formally singular evolution equations can be regularized at $\mathscr{I}^+$. In section 3 we describe our numerical method for solving these equations. The numerical results are presented in section 4. As a first test problem we evolve Schwarzschild spacetime and demonstrate the convergence of the numerical solution. Next, a gravitational perturbation is included. A regular expression at $\mathscr{I}^+$ for the Bondi news function [9] describing the outgoing gravitational radiation is derived and evaluated numerically. We conclude and discuss possible directions for future work in section 5.

2. Formulation

2.1. Definitions and gauge choices

We assume that spacetime is axisymmetric with Killing vector ξ. For simplicity we also assume here that ξ is hypersurface orthogonal. Spherical polar coordinates t, r, θ, ϕ are chosen such that $\xi = \partial/\partial\phi$.

The spacetime metric ${}^{(4)}g_{\alpha\beta}$ is written as

$$ {}^{(4)}g_{\alpha\beta} = \psi^{-2}\,{}^{(4)}\gamma_{\alpha\beta}, \tag{1} $$

where ψ is the conformal factor and ${}^{(4)}\gamma_{\alpha\beta}$ the conformal metric. Greek indices $\alpha, \beta, \ldots$ are spacetime indices (t, r, θ, ϕ). The conformal factor ψ is positive and approaches zero at future null infinity, which we put at a fixed coordinate location $r = 1$. The conformal metric ${}^{(4)}\gamma_{\alpha\beta}$ is assumed to be regular there.

We decompose the metric in ADM form as

$$ {}^{(4)}g_{\alpha\beta}\mathrm{d}x^\alpha \mathrm{d}x^\beta = -\alpha^2 \mathrm{d}t^2 + g_{ij}(\mathrm{d}x^i + \beta^i \mathrm{d}t)(\mathrm{d}x^j + \beta^j \mathrm{d}t), \tag{2} $$

where g_{ij} is the spatial metric, α the lapse function and β^i the shift vector. Latin indices $i, j, \ldots$ are spatial (r, θ, ϕ). Similarly, we write the conformal spacetime metric as

$$ {}^{(4)}\gamma_{\alpha\beta}\mathrm{d}x^\alpha \mathrm{d}x^\beta = -\tilde{\alpha}^2 \mathrm{d}t^2 + \gamma_{ij}(\mathrm{d}x^i + \beta^i \mathrm{d}t)(\mathrm{d}x^j + \beta^j \mathrm{d}t), \tag{3} $$

where $\gamma_{ij} = \psi^2 g_{ij}$ is the conformal spatial metric and $\tilde{\alpha} = \psi\alpha$ the conformal lapse.

The spatial coordinates are chosen such that $\beta^\phi = 0$ and the conformal spatial metric takes the form

$$\gamma_{ij}\mathrm{d}x^i\mathrm{d}x^j = \mathrm{e}^{2\eta\sin\theta}(\mathrm{d}r^2 + r^2\mathrm{d}\theta^2) + r^2\sin^2\theta\,\mathrm{d}\phi^2. \tag{4}$$

This is sometimes called *quasi-isotropic gauge*. We note that this choice of gauge differs from the spatial harmonic gauge used in [23].‡

The extrinsic curvature is defined by

$$\partial_t g_{ij} = -2\alpha K_{ij} + \mathcal{L}_\beta g_{ij}, \tag{5}$$

where $\mathcal{L}$ denotes the Lie derivative. Preservation of the conditions $g_{\theta\theta} = r^2 g_{rr}$ and $g_{r\theta} = 0$ under the evolution equation (5) implies

$$\beta^r{}_{,r} - \beta^\theta{}_{,\theta} - r^{-1}\beta^r = \alpha(K^r{}_r - K^\theta{}_\theta) \equiv \tilde{\alpha}\tilde{U}, \tag{6}$$

$$\beta^r{}_{,\theta} + r^2\beta^\theta{}_{,r} = 2\alpha K^r{}_\theta \equiv 2\tilde{\alpha}\tilde{K}^r{}_\theta. \tag{7}$$

Similarly as in [25] we have defined the following components of the extrinsic curvature,

$$K^r{}_r - K^\theta{}_\theta \equiv \psi\tilde{U}, \qquad K^r{}_\theta = r^{-2}K^\theta{}_r \equiv \psi\tilde{K}^r{}_\theta, \tag{8}$$

and, motivated by regularity concerns on the axis of symmetry [25, 26, 27], we also set

$$K^\theta{}_\theta - K^\phi{}_\phi \equiv \psi\sin\theta\,\tilde{W}. \tag{9}$$

It is easy to see that the quantities $\tilde{U}$, $\tilde{K}^r{}_\theta$ and $\tilde{W}$ defined in (8) and (9) have the same conformal weight as the traceless momentum

$$\pi^{\mathrm{tr}\,ij} = \sqrt{g}(K^{ij} - \tfrac{1}{3}g^{ij}K_l{}^l) \tag{10}$$

used in [23], where g denotes the determinant of g_{ij}. Note also that because $\tilde{K}^r{}_\theta$, $\tilde{W}$ and $\tilde{U}$ are either off-diagonal or differences of diagonal components of the extrinsic curvature, they can in fact be regarded as the three independent components of the *traceless* part of the extrinsic curvature in our case.

As in [23] we require the time slices to have constant mean curvature,

$$g^{ij}K_{ij} \equiv -K = \text{const}. \tag{11}$$

Note the slightly awkward sign in the definition of the constant K; with our sign convention for the extrinsic curvature (5) we require K to be *positive* so that the slices reach *future* null infinity. Preservation of (11) under the Einstein evolution equation for the extrinsic curvature yields the following elliptic equation for the conformal lapse,

$$\begin{aligned} 0 = {} & \tilde{\alpha}_{,rr} + 2r^{-1}\tilde{\alpha}_{,r} + r^{-2}(\tilde{\alpha}_{,\theta\theta} + \tfrac{c}{s}\tilde{\alpha}_{,\theta}) \\ & -\tfrac{1}{2}s\tilde{\alpha}(\eta_{,rr} + r^{-1}\eta_{,r} + r^{-2}\eta_{,\theta\theta} + 2r^{-2}\tfrac{c}{s}\eta_{,\theta} - r^{-2}\eta) \\ & +\tfrac{3}{2}\tilde{\alpha}\left[P_r(P_r - 2\tilde{A}_r) + r^{-2}P_\theta(P_\theta - 2\tilde{A}_\theta)\right] - \tfrac{1}{6}\psi^{-2}\tilde{\alpha}\mathrm{e}^{2s\eta}K^2 \\ & -\tfrac{5}{2}\tilde{\alpha}\mathrm{e}^{2s\eta}\left[\tfrac{1}{3}(\tilde{U} + \tfrac{1}{2}s\tilde{W})^2 + \tfrac{1}{4}(s\tilde{W})^2 + r^{-2}(\tilde{K}^r{}_\theta)^2\right]. \end{aligned} \tag{12}$$

Here and in the following we use the abbreviations

$$s \equiv \sin\theta, \quad c \equiv \cos\theta, \quad P_B \equiv \psi^{-1}\psi_{,B}, \quad \tilde{A}_B \equiv \tilde{\alpha}^{-1}\tilde{\alpha}_{,B}, \tag{13}$$

upper-case Latin indices $A, B, \ldots$ ranging over r and θ.

‡ It is, in a sense, its two-dimensional analogue: if we define a two-dimensional metric H_{AB} by the part of the line element (4) orthogonal to the Killing vector, $H_{AB}\mathrm{d}x^A\mathrm{d}x^B = \mathrm{e}^{2\eta\sin\theta}(\mathrm{d}r^2 + r^2\mathrm{d}\theta^2)$, then $V^C \equiv H^{AB}(\Gamma^C{}_{AB} - \mathring{\Gamma}^C{}_{AB}) = 0$, where $\Gamma^C{}_{AB}$ are the Christoffel symbols of H_{AB} and $\mathring{\Gamma}^C{}_{AB}$ are the Christoffel symbols of the flat metric (H_{AB} with $\eta = 0$). [The author thanks V. Moncrief for pointing this out.]

2.2. Constraint and evolution equations

As usual in ADM-like reductions, the Einstein equations split into constraint and evolution equations. The Hamiltonian constraint is

$$\begin{aligned}0 = \psi_{,rr} + 2r^{-1}\psi_{,r} + r^{-2}(\psi_{,\theta\theta} + \tfrac{c}{s}\psi_{,\theta}) - \tfrac{3}{2}\psi^{-1}\left[(\psi_{,r})^2 + r^{-2}(\psi_{,\theta})^2\right] \\ -\tfrac{1}{2}s\psi(\eta_{,rr} + r^{-1}\eta_{,r} + r^{-2}\eta_{,\theta\theta} + 2r^{-2}\tfrac{c}{s}\eta_{,\theta} - r^{-2}\eta) \\ -\tfrac{1}{2}\psi \mathrm{e}^{2s\eta}\left[\tfrac{1}{3}(\tilde{U} + \tfrac{1}{2}s\tilde{W})^2 + \tfrac{1}{4}(s\tilde{W})^2 + r^{-2}(\tilde{K}^r{}_\theta)^2\right] \\ +\tfrac{1}{6}\psi^{-1}\mathrm{e}^{2s\eta}K^2. \end{aligned} \tag{14}$$

The momentum constraints are

$$\begin{aligned}0 = \mathcal{C}^r \equiv \tfrac{2}{3}\tilde{U}_{,r} + \tfrac{1}{3}s\tilde{W}_{,r} + r^{-2}\tilde{K}^r{}_{\theta,\theta} + r^{-2}\tilde{K}^r{}_\theta(\tfrac{c}{s} + 2c\eta + 2s\eta_{,\theta} - 2P_\theta) \\ +\tilde{U}(s\eta_{,r} - \tfrac{4}{3}P_r + 2r^{-1}) + s\tilde{W}(r^{-1} - \tfrac{2}{3}P_r), \end{aligned} \tag{15}$$

$$\begin{aligned}0 = \mathcal{C}^\theta \equiv -\tfrac{1}{3}\tilde{U}_{,\theta} + \tfrac{1}{3}s\tilde{W}_{,\theta} + \tilde{K}^r{}_{\theta,r} + 2\tilde{K}^r{}_\theta(s\eta_{,r} - P_r + r^{-1}) \\ +\tilde{U}(-c\eta - s\eta_{,\theta} + \tfrac{2}{3}P_\theta) + \tilde{W}(\tfrac{4}{3}c - \tfrac{2}{3}sP_\theta). \end{aligned} \tag{16}$$

We have the following evolution equations,

$$\psi_{,t} = \beta^r\psi_{,r} + \beta^\theta\psi_{,\theta} - (\tfrac{c}{s}\beta^\theta + r^{-1}\beta^r) - \tfrac{1}{3}\tilde{\alpha}(K + \psi(\tilde{U} + 2s\tilde{W}), \tag{17}$$

$$\eta_{,t} = \beta^r\eta_{,r} + \beta^\theta\eta_{,\theta} + \tfrac{c}{s}\beta^\theta\eta + (s^{-1}\beta^\theta)_{,\theta} - \tilde{\alpha}\tilde{W}, \tag{18}$$

$$\begin{aligned}\tilde{W}_{,t} = \beta^r\tilde{W}_{,r} + \beta^\theta\tilde{W}_{,\theta} + (2\tfrac{c}{s}\beta^\theta + r^{-1}\beta^r)\tilde{W} \\ +\mathrm{e}^{-2s\eta}r^{-2}\left[-(s^{-1}\tilde{\alpha}_{,\theta})_{,\theta} + 2\tilde{\alpha}\psi^{-1}(s^{-1}\psi_{,\theta})_{,\theta}\right] \\ -\tilde{\alpha}\mathrm{e}^{-2s\eta}\big\{\eta_{,rr} + 2r^{-1}\eta_{,r} + r^{-2}[\eta_{,\theta\theta} - \eta + c(s^{-1}\eta)_{,\theta}] \\ +(\tilde{A}_r - 2P_r)\eta_{,r} - r^{-2}s^{-1}(\tilde{A}_\theta - 2P_\theta)(s\eta_{,\theta} + c\eta)\big\} \\ -2s^{-1}\tilde{K}^r{}_\theta\beta^\theta{}_{,r} + \tfrac{2}{3}\tilde{\alpha}s^{-1}\left[s\tilde{W}(s\tilde{W} + \tfrac{1}{2}\tilde{U} - \psi^{-1}K) + 3r^{-2}(\tilde{K}^r{}_\theta)^2\right] \end{aligned} \tag{19}$$

$$\begin{aligned}\tilde{K}^r{}_{\theta,t} = \beta^r\tilde{K}^r{}_{\theta,r} + \beta^\theta\tilde{K}^r{}_{\theta,\theta} + \tfrac{c}{s}\beta^\theta\tilde{K}^r{}_\theta + \mathrm{e}^{-2s\eta}(-\tilde{\alpha}_{,r\theta} + 2\tilde{\alpha}\psi^{-1}\psi_{,r\theta}) \\ +\tilde{\alpha}\mathrm{e}^{-2s\eta}\big[(\tilde{A}_r - 2P_r + r^{-1})(s\eta_{,\theta} + c\eta) + (\tilde{A}_\theta - 2P_\theta)(s\eta_{,r} + r^{-1}) \\ +c\eta_{,r}\big] + \tfrac{2}{3}\tilde{\alpha}\tilde{K}^r{}_\theta(s\tilde{W} - \psi^{-1}K + 2\tilde{U}) - r^2\beta^\theta{}_{,r}\tilde{U}, \end{aligned} \tag{20}$$

$$\begin{aligned}\tilde{U}_{,t} = \beta^r\tilde{U}_{,r} + \beta^\theta\tilde{U}_{,\theta} + \tilde{U}(\tfrac{c}{s}\beta^\theta + r^{-1}\beta^r) \\ +\mathrm{e}^{-2s\eta}[-\tilde{\alpha}_{,rr} + r^{-2}\tilde{\alpha}_{,\theta\theta} + 2\tilde{\alpha}\psi^{-1}(\psi_{,rr} - r^{-2}\psi_{,\theta\theta})] \\ +\tilde{\alpha}\mathrm{e}^{-2s\eta}[(\tilde{A}_r - 2P_r)(2s\eta_{,r} + r^{-1}) + 2sr^{-1}\eta_{,r} \\ -2r^{-2}(\tilde{A}_\theta - 2P_\theta)(s\eta_{,\theta} + c\eta + \tfrac{c}{s})] \\ +\tfrac{1}{3}\tilde{\alpha}\tilde{U}(2s\tilde{W} - 2\psi^{-1}K + \tilde{U}) + 4\tilde{K}^r{}_\theta(\beta^\theta{}_{,r} - \tilde{\alpha}r^{-2}\tilde{K}^r{}_\theta). \end{aligned} \tag{21}$$

We observe that all the equations are manifestly regular at the axis of symmetry $\theta = 0$ when the parities of the fields with respect to $\theta = 0$ are taken into account (table 1). These can be inferred from the general behaviour of regular axisymmetric tensor fields [28].

2.3. Partially constrained evolution and hyperbolicity

We determine the conformal factor ψ by solving the momentum constraint (14) rather than the evolution equation (17). On the other hand, the extrinsic curvature variables $\tilde{W}, \tilde{K}^r{}_\theta$ and $\tilde{U}$ are evolved using the evolution equations (19)–(21) and the

Table 1. Angular parities of the fundamental variables: even (+) or odd (−). The parities about $\theta = 0$ follow from regularity on axis, those about $\theta = \pi/2$ from the reflection symmetry we impose.

Variable	$\tilde{\alpha}$	β^r	β^θ	ψ	η	$\tilde{W}$	$\tilde{K}^r{}_\theta$	$\tilde{U}$
$\theta = 0$	+	+	−	+	−	−	−	+
$\theta = \pi/2$	+	+	−	+	+	+	−	+

momentum constraints (15) and (16) are not solved explicitly. Hence we adopt a partially constrained evolution scheme.

Of course the constraints are preserved by the evolution equations, which imply the following subsidiary system,

$$\mathcal{C}^t{}_{,t} \simeq \beta^r \mathcal{C}^t{}_{,r} + \beta^\theta \mathcal{C}^t{}_{,\theta} - \tfrac{1}{2}\tilde{\alpha}\psi(\mathcal{C}^r{}_{,r} + r^{-2}\mathcal{C}^\theta{}_{,\theta}), \tag{22}$$

$$\mathcal{C}^r{}_{,t} \simeq \beta^r \mathcal{C}^r{}_{,r} + \beta^\theta \mathcal{C}^r{}_{,\theta} + \tfrac{4}{3}\mathrm{e}^{-2s\eta}\tilde{\alpha}\psi^{-1}\mathcal{C}^t{}_{,r}, \tag{23}$$

$$\mathcal{C}^\theta{}_{,r} \simeq \beta^r \mathcal{C}^\theta{}_{,r} + \beta^\theta \mathcal{C}^\theta{}_{,\theta} + \tfrac{4}{3}\mathrm{e}^{-2s\eta}\tilde{\alpha}\psi^{-1}\mathcal{C}^t{}_{,\theta}, \tag{24}$$

$$\tag{25}$$

where the symbol $\simeq$ signifies that only the principal parts have been displayed, and the remaining terms are homogeneous in the constraints. If the Hamiltonian constraint is enforced exactly, $\mathcal{C}^t = 0$, then the remaining evolution equations for $\mathcal{C}^r$ and $\mathcal{C}^\theta$ are clearly hyperbolic (they are advection equations along the shift). If the Hamiltonian constraint is not enforced then the full constraint evolution system is *not* hyperbolic (the characteristic speeds

$$\lambda^r = \beta^r \pm \sqrt{\tfrac{2}{3}}\,\mathrm{e}^{-s\eta}\tilde{\alpha}\,\mathrm{i}, \qquad \lambda^\theta = \beta^\theta \pm \sqrt{\tfrac{2}{3}}\,r^{-1}\mathrm{e}^{-s\eta}\tilde{\alpha}\,\mathrm{i} \tag{26}$$

are complex). This might be cured by adding multiples of the Hamiltonian constraint to the evolution equations; however, we have not found such a constraint addition that both yields a hyperbolic constraint evolution system and is compatible with regularity of the main evolution equations on the axis of symmetry. Hence a free evolution scheme that solves none of the constraint equations during the evolution does not appear to be feasible. However, our formulation includes three elliptic equations for the gauge variables $\tilde{\alpha}$ and β^A anyway and solving one additional elliptic equation for the conformal factor is not overly expensive.

If we assume that $\tilde{\alpha}, \beta^A$ and ψ are given by the solution of the elliptic equations, then the pair of evolution equations (18) and (19) forms a wave equation to principal parts,

$$(\partial_t - \beta^A\partial_A)^2\eta \simeq \tilde{\alpha}^2\mathrm{e}^{-2s\eta}(\eta_{,rr} + r^{-2}\eta_{,\theta\theta}), \tag{27}$$

and the evolution equations (20) and (21) are advection equations along the shift to principal parts. Hence the evolution equations are hyperbolic. A rigorous proof of the well posedness of the present mixed elliptic-hyperbolic hyperboloidal initial value problem remains to be carried out. For a similar mixed elliptic-hyperbolic formulation on a Cauchy foliation, such a proof was given in in [29].

2.4. Regularity at future null infinity

The CMC slicing condition (12), the constraint equations (14)–(16) and the evolution equations for the extrinsic curvature (19)–(21) are formally singular at $\mathscr{I}^+$, where

the conformal factor ψ vanishes. Our elliptic solver (section 3.4) is well adapted to such degenerate elliptic equations. However, the right-hand sides of the evolution equations cannot be evaluated at $\mathscr{I}^+$ in their present form. In [23] two methods for obtaining regular forms of the evolution equations at $\mathscr{I}^+$ were presented: the first based on Taylor expansions, the second on an argument due to Penrose [30]. For the numerical results presented in section 4 we followed the second approach but we have also implemented the first approach, as discussed further below.

Penrose showed that provided certain smoothness assumptions hold (in particular, the conformal metric must be C^3 up to the boundary), the conformal Weyl tensor (i.e., corresponding to the conformal metric ${}^{(4)}\gamma_{\alpha\beta}$) vanishes at $\mathscr{I}^+$. This implies [23] that the electric part of the *physical* Weyl tensor (i.e., corresponding to ${}^{(4)}g_{\alpha\beta}$) also vanishes at $\mathscr{I}^+$,

$$E_{\alpha\gamma} = n^\beta n^\delta C_{\alpha\beta\gamma\delta}[{}^{(4)}g] \mathrel{\hat{=}} 0, \tag{28}$$

where n^α is the unit normal to the $t = \text{const}$ slices and $\mathrel{\hat{=}}$ denotes equality at $\mathscr{I}^+$. It is straightforward to compute the Weyl tensor for the metric ${}^{(4)}\gamma_{\alpha\beta}$ defined in (3) and (4). Any time derivatives are substituted using the evolution equations. (Here a computer algebra program is very useful; we used REDUCE [31].) Setting $E_{\alpha\gamma} \mathrel{\hat{=}} 0$ immediately gives regular expressions for the formally singular terms in (19)–(21). Thus we obtain the following manifestly regular evolution equations at $\mathscr{I}^+$,

$$\begin{aligned}
\tilde{W}_{,t} \mathrel{\hat{=}} {} & \beta^r \tilde{W}_{,r} + \beta^\theta \tilde{W}_{,\theta} + (2\tfrac{c}{s}\beta^\theta + r^{-1}\beta^r)\tilde{W} - \mathrm{e}^{-2s\eta} r^{-2}(s^{-1}\tilde{\alpha}_{,\theta})_{,\theta} \\
& + \tilde{\alpha}\mathrm{e}^{-2s\eta}\big\{\eta_{,rr} + 2r^{-1}\eta_{,r} + r^{-2}[\eta_{,\theta\theta} - \eta + c(s^{-1}\eta)_{,\theta}] \\
& \qquad - A_r\eta_{,r} + r^{-2}s^{-1}A_\theta(s\eta_{,\theta} + c\eta)\big\} \\
& - 2s^{-1}\tilde{K}^r{}_\theta \beta^\theta{}_{,r} + \tilde{\alpha}[4s^{-1}r^{-2}(\tilde{K}^r{}_\theta)^2 - \tilde{U}\tilde{W}],
\end{aligned} \tag{29}$$

$$\begin{aligned}
\tilde{K}^r{}_{\theta,t} \mathrel{\hat{=}} {} & \beta^r \tilde{K}^r{}_{\theta,r} + \beta^\theta \tilde{K}^r{}_{\theta,\theta} + \tfrac{c}{s}\beta^\theta \tilde{K}^r{}_\theta - \mathrm{e}^{-2s\eta}\tilde{\alpha}_{,r\theta} \\
& + \tilde{\alpha}\mathrm{e}^{-2s\eta}\big[(\tilde{A}_r - r^{-1})(s\eta_{,\theta} + c\eta) + \tilde{A}_\theta(s\eta_{,r} + r^{-1}) - c\eta_{,r}\big] \\
& + 2\tilde{\alpha}\tilde{K}^r{}_\theta(s\tilde{W} + \tilde{U}) - r^2\beta^\theta{}_{,r}\tilde{U},
\end{aligned} \tag{30}$$

$$\begin{aligned}
\tilde{U}_{,t} \mathrel{\hat{=}} {} & \beta^r \tilde{U}_{,r} + \beta^\theta \tilde{U}_{,\theta} + \tilde{U}(\tfrac{c}{s}\beta^\theta + r^{-1}\beta^r) + \mathrm{e}^{-2s\eta}(-\tilde{\alpha}_{,rr} + r^{-2}\tilde{\alpha}_{,\theta\theta}) \\
& + \tilde{\alpha}\mathrm{e}^{-2s\eta}[\tilde{A}_r(2s\eta_{,r} + r^{-1}) - 2r^{-2}(\tilde{A}_\theta - \tfrac{c}{s})(s\eta_{,\theta} + c\eta) - 2sr^{-1}\eta_{,r}] \\
& + \tilde{\alpha}\tilde{U}(2s\tilde{W} + \tilde{U}) + 4\tilde{K}^r{}_\theta(\beta^\theta{}_{,r} - \tilde{\alpha}r^{-2}\tilde{K}^r{}_\theta).
\end{aligned} \tag{31}$$

The other approach to regularity at $\mathscr{I}^+$ discussed in [23] is based on an expansion of all the fields in (finite) Taylor series with respect to radius r about $\mathscr{I}^+$. Substituting these expansions in the singular constraint equations, one obtains conditions on the fields and their radial derivatives that can be used in order to evaluate the formally singular terms in the evolution equations. This approach is more general in that it does not require Penrose's smoothness assumption.

As necessary conditions for a regular evolution at $\mathscr{I}^+$, we obtained in [23] a set of conditions that had been discovered in [32], namely that the shear of $\mathscr{I}^+$ and the radial components $\pi^{\mathrm{tr}\,ri}$ of the traceless momentum vanish. In the axisymmetric formulation we consider here, these conditions read

$$\tilde{W} \mathrel{\hat{=}} -\mathrm{e}^{-s\eta}\eta_{,r}, \qquad \tilde{U} \mathrel{\hat{=}} \tfrac{1}{2}\mathrm{e}^{-s\eta}s\eta_{,r}, \qquad \tilde{K}^r{}_\theta \mathrel{\hat{=}} 0. \tag{32}$$

One might be tempted to impose these conditions as Dirichlet conditions on the extrinsic curvature at $\mathscr{I}^+$, thus avoiding to evaluate the singular evolution equations there. However, numerical evolutions with these Dirichlet boundary conditions were

found to be unstable. This is perhaps not surprising because at $\mathscr{I}^+$ all the fields are purely outgoing and hence imposing boundary conditions there is ill posed (although of course the conditions (32) are satisfied for a *given* solution of the field equations). It is worthwhile to observe though, as we already did in [23], that the evolution equations (19)–(21) contain remarkable damping terms that cause potential violations of the regularity conditions (32) to decay exponentially in the neighbourhood of $\mathscr{I}^+$:

$$u_{,t} = \ldots - \tfrac{2}{3}\tilde{\alpha}\psi^{-1}Ku \tag{33}$$

for each $u \in \{\tilde{W}, \tilde{K}^r{}_\theta, \tilde{U}\}$. The term has the "right sign" because $K > 0$.

Instead of imposing the regularity conditions (32) directly, however, we can extract more information from the Taylor expansions that allows us to evaluate the singular terms in the evolution equations directly [23]. The resulting modified evolution equations at $\mathscr{I}^+$ are detailed for the current axisymmetric scheme in Appendix B. Their main difference to (29)–(31) lies in the presence of terms involving first radial derivatives of the extrinsic curvature at $\mathscr{I}^+$ (cf. equation (B.9)). We found this version of the evolution equations at $\mathscr{I}^+$ to be numerically stable as well, and the results agree with those in section 4 within numerical error (see Appendix B for details).

It is worth noting here that the quasi-isotropic spatial gauge we use differs from the spatially harmonic gauge of [23]. Nevertheless, we were able to apply the same procedure for evaluating the formally singular terms at $\mathscr{I}^+$. This provides some substance to the claim in [23] that the precise form of the spatial gauge conditions is inessential for the method to be applicable.

3. Numerical method

Having obtained a set of gauge conditions, constraints and evolution equations, we now describe how we solve them numerically. First we summarize the evolution scheme, i.e. which variables are evolved using which equations. Next we specify our choice for the computational domain and the discretization of the partial differential equations. We then focus on the two main aspects of the code, the time integration scheme and the elliptic solver. The code has been written in C++. Unless otherwise indicated all routines have been developed from scratch.

3.1. Evolution scheme

Our fundamental variables are $\tilde{\alpha}, \beta^A, \psi, \eta, \tilde{W}, \tilde{K}^r{}_\theta$ and $\tilde{U}$. The variables $\eta, \tilde{W}, \tilde{K}^r{}_\theta$ and $\tilde{U}$ are evolved using the evolution equations (18)–(21). At each time step we solve the CMC slicing condition (12) for $\tilde{\alpha}$, the quasi-isotropic gauge conditions (6) and (7) for β^A, and the Hamiltonian constraint (14) for ψ. Details on how the quasi-isotropic gauge conditions are treated are given in Appendix A.1. The momentum constraints are only solved initially (Appendix A.2).

3.2. Domain and discretization

For the applications considered in this paper, the spatial numerical domain is taken to be the quarter of an annulus, $r_{\min} \leqslant r \leqslant 1$ and $0 \leqslant \theta \leqslant \pi/2$. The inner boundary at $r = r_{\min}$ will be taken to lie within a black hole event horizon (black hole excision), and the outer boundary at $r = 1$ corresponds to $\mathscr{I}^+$. The axis of symmetry is at $\theta = 0$, and we impose an additional reflection symmetry about the plane $\theta = \pi/2$.

The fields typically have the steepest gradients close to the black hole and hence it is advisable to use a non-uniform radial grid in order to provide more numerical resolution towards the inner boundary. We introduce a quadratic map

$$r(x) = Qx^2 + (1 - r_{\min} - Q)x + r_{\min}, \tag{34}$$

where $0 \leqslant Q < 1$ is a constant. This map satisfies $r(0) = r_{\min}$ and $r(1) = 1$. We use a uniform grid in x, i.e. we place grid points at $x_i = i/N_r$, $0 \leqslant i \leqslant N_r$, where N_r is the number of radial grid points. Note in particular that there are grid points right at the inner boundary and at $\mathscr{I}^+$. In the angular direction we use a uniform staggered grid: $\theta_j = \frac{\pi}{2}(j - \frac{1}{2})/N_\theta$, $1 \leqslant i \leqslant N_\theta$. Two layers of ghost points are added on either side, corresponding to $j = -1, 0$ and $j = N_{\theta+1}, N_{\theta+2}$. Values at these ghost points are set according to the angular parities of the various fields, which are listed in table 1. E.g. for a field u that is odd about $\theta = 0$ we set $u_{i0} = -u_{i,1}$ and $u_{i,-1} = -u_{i2}$, and for an even field we set $u_{i0} = u_{i,1}$ and $u_{i,-1} = u_{i2}$. Here u_{ij} denotes the value of u at the grid point with indices (i, j).

The spatial derivatives are discretized using fourth-order accurate finite differences. One-sided differences are used in the radial direction at the boundaries; everywhere else centred differences are used (see Appendix C for details).

3.3. Time integration

A fourth-order Runge-Kutta method is used in order to integrate the evolution equations forward in time. At each substep of this method, the elliptic equations are solved as described below in section 3.4. Since all the characteristics point towards the exterior of the domain both at the inner excision boundary and at $\mathscr{I}^+$, no boundary conditions are imposed there—the evolution equations are discretized using one-sided finite differences. At $\mathscr{I}^+$ the evolution equations (19)–(21) for the extrinsic curvature are replaced with their regularized versions (29)–(31). Kreiss-Oliger dissipation [33] is added in order to ensure stability (Appendix C). No modifications to the dissipation operators or special smoothing operations at $\mathscr{I}^+$ have been required.

3.4. Elliptic solver and boundary conditions

The elliptic equations are solved by means of a multigrid method [34, 35] using Full Approximation Storage (FAS). Because of the singular nature of the equations at $\mathscr{I}^+$ ($r = 1$), we have found it necessary to use line relaxation in the radial direction, i.e. all points on a line $\theta = \text{const}$ are solved simultaneously. With our fourth-order finite-difference discretization this requires solving a penta-diagonal linear system of equations, for which a fast algorithm exist (we use the routines `bandec` and `banbks` in [36]). For the Hamiltonian constraint (14) an outer Newton-Raphson iteration is employed for each such line solve; all remaining elliptic equations are linear. The lines $\theta = \text{const}$ are then traversed and updated in ascending order $j = 1, 2, \ldots, N_\theta$ (Gauss-Seidel relaxation in the θ-direction). We have found this method to be very robust and effective, leading to a reduction of the residual of about an order of magnitude per W-cycle. No problems with convergence at the singular boundary were encountered.

The elliptic equations require boundary conditions at the inner $r = r_{\min}$ and outer $r = 1$ boundary (in addition to the parity boundary conditions at $\theta = 0, \pi/2$), which we shall now specify.

At the outer boundary ($\mathscr{I}^+$) we take the angular shift to vanish, $\beta^\theta \mathrel{\hat{=}} 0$. The conformal factor vanishes there by definition, $\psi \mathrel{\hat{=}} 0$. Preservation of this condition under the evolution equation (17) yields a boundary condition for the conformal lapse,

$$\tilde{\alpha} \mathrel{\hat{=}} -\mathrm{e}^{s\eta}\beta^r. \tag{35}$$

We remark that these boundary conditions for the lapse and shift ensure that the normal n^α to the time slices is null at $\mathscr{I}^+$. The radial shift β^r appearing in (35) cannot be chosen freely but is determined by the quasi-isotropic gauge conditions. After each Gauss-Seidel relaxation sweep we integrate (7) along the boundary to determine β^r there. The integration constant can be fixed e.g. by requiring that the average of β^r along the boundary agree with the value obtained from the exact Schwarzschild solution that we consider in section 4.

At the inner excision boundary, we also take β^θ to vanish, and we freeze $\tilde{\alpha}$ to the value corresponding to the exact Schwarzschild solution. However, the conformal factor ψ *cannot* be chosen freely. This is because ψ obeys an evolution equation with outgoing characteristic speed at the excision boundary, equation (17). In order to determine the correct value of ψ there, we keep a copy of ψ that is evolved using (17). At the end of each timestep this copy of ψ is reset to agree with the solution of the Hamiltonian constraint. This procedure was found to be crucial for ensuring that the *momentum* constraints are preserved during the numerical evolution.

4. Numerical results

In this section, we apply our code to the evolution of a (perturbed) Schwarzschild black hole. First we focus on the unperturbed Schwarzschild solution and demonstrate that long-term stable and convergent evolutions can be obtained. Next we include a small gravitational perturbation. The outgoing gravitational radiation as represented by the Bondi news function is computed at $\mathscr{I}^+$.

4.1. Schwarzschild spacetime

First we describe how the exact solution is computed, which is needed both for the boundary conditions of some of the elliptic equations (section 3.4) and in order to compare with the numerical solution during the evolution. The Schwarzschild solution in CMC slicing was derived in [37, 38]. Its line element is

$$ds^2 = -\left(1-\frac{2M}{\bar{r}}\right)\mathrm{d}t^2 + \frac{1}{f^2}\,\mathrm{d}\bar{r}^2 - \frac{2a}{f}\,dt\,\mathrm{d}\bar{r} + \bar{r}^2(\mathrm{d}\theta^2 + \sin^2\theta\,\mathrm{d}\phi^2), \tag{36}$$

where

$$f(\bar{r}) = \left(1-\frac{2M}{\bar{r}}+a^2\right)^{1/2}, \qquad a(\bar{r}) = \frac{K\bar{r}}{3} - \frac{C}{\bar{r}^2}, \tag{37}$$

and M (mass), K (mean curvature) and C are constants.

As in [24] we introduce a new radial coordinate r (the coordinate used in our evolution scheme) by requiring the spatial metric to be conformally flat in the new coordinates. Hence r obeys

$$\frac{\mathrm{d}r}{\mathrm{d}\bar{r}} = \frac{r}{\bar{r}f(\bar{r})}. \tag{38}$$

This ordinary differential equation is integrated numerically to high precision using Mathematica. The boundary condition is that $r \to 1$ as $\bar{r} \to \infty$.

The metric variables defined in section 2.1 are then given by

$$\psi = \frac{r}{\bar{r}}, \quad \tilde{\alpha} = \frac{rf}{\bar{r}}, \quad \beta^r = -\frac{ra}{\bar{r}}, \quad \beta^\theta = 0, \quad \eta = 0. \tag{39}$$

The extrinsic curvature variables are found to be

$$\tilde{U} = -\frac{3C}{\bar{r}^2 r}, \quad \tilde{W} = 0, \quad \tilde{K}^r{}_\theta = 0, \tag{40}$$

and the vector V^A introduced in order to solve the momentum constraints initially (Appendix A.2) is

$$V^r = \frac{C}{r^2}, \quad V^\theta = 0. \tag{41}$$

For the numerical evolutions presented in this paper we choose $M = 1$, $K = 1/2$ and $C = 2$ (although we have obtained stable evolutions across a wide range of parameter values). The inner boundary is placed at $r_{\min} = 0.05$, just inside the horizon at $\bar{r} = 2 \Leftrightarrow r = 0.0635$.

We run the simulation with two different numerical resolutions $(N_r, N_\theta) = (64, 8)$ and $(128, 16)$. The radial grid is nonuniform with $Q = 3/4$ in (34) in both cases.

The time step Δt is limited by the Courant-Friedrichs-Lewy condition

$$\Delta t < \min\left(\frac{\Delta r}{|v^r_\pm|}, \frac{\Delta\theta}{|v^\theta_\pm|}\right), \tag{42}$$

where Δr is the grid spacing and $v^r_\pm$ are the incoming and outgoing characteristic speeds of the evolution system (17)–(21) in the r-direction (similarly in the θ-direction), and the minimum is taken over all grid points. For our choice of parameters the time step is constrained by the outgoing radial characteristic speed at $\mathscr{I}^+$,

$$v^r_+ = -\beta^r + \mathrm{e}^{-s\eta}\tilde{\alpha} \mathrel{\hat{=}} \frac{2K}{3} \tag{43}$$

for the Schwarzschild solution. The time step is taken to be about 3/4 of the maximum allowed value computed in this way: for the lower resolution we use $\Delta t = 0.06$.

During the evolution, we compute the difference of the numerical solution with respect to the exact solution for each of the evolved variables and take its discrete L_2 norm. This is divided by the norm of the exact solution for the corresponding variable whenever the latter does not vanish. Of these results a vector 2-norm (square root of the sum of the squares) is taken. The resulting quantity represents a measure of the overall relative error of the numerical solution as a function of time and is plotted in figure 1. The error grows only linearly with time. It decreases by a factor of about 15 on average as the resolution is doubled, close to the expected convergence factor of $2^4 = 16$ for a fourth-order accurate scheme. The main contribution to the error comes from the region close to the black hole horizon where the fields have the steepest gradients. The numerical solution remains smooth all the way up to $\mathscr{I}^+$ during the entire evolution.

4.2. Perturbed Schwarzschild spacetime

Next, we include a small gravitational perturbation in our evolutions. This is done by taking the variable η, which vanishes for the exact Schwarzschild solution, to be a Gaussian initially,

$$\eta = A \sin\theta \, \exp\left[-\frac{(r - r_c)^2}{2\sigma^2}\right]. \tag{44}$$

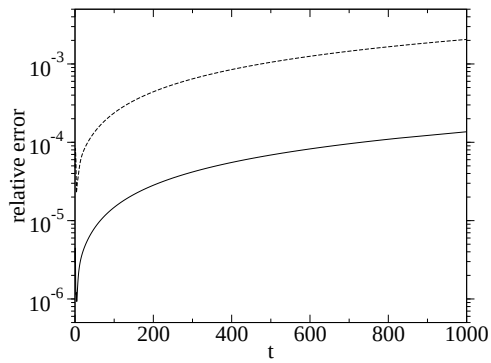

Figure 1. Relative error of the numerical solution with respect to the exact solution for an evolution of Schwarzschild spacetime, computed as described in the text. Two different numerical resolutions are shown, $(N_r, N_\theta) = (64, 8)$ (dashed line) and $(128, 16)$ (solid line).

The factor $\sin\theta$ has been included for parity reasons (table 1). We choose $A = 10^{-4}$, $r_c = 0.5$ and $\sigma = 0.05$. We stress that these initial data are evolved with the full nonlinear Einstein equations. The linearized problem has been studied extensively; in particular, numerical evolutions of the Bardeen-Press equation [39] and the Regge-Wheeler-Zerilli equations [40] have been performed on hyperboloidal slices.

In order to demonstrate the consistency and convergence of our code, we monitor the momentum constraints, which are not solved explicitly during the evolution. For the unperturbed Schwarzschild solution, each term in the θ-momentum constraint (16) vanishes separately. This is not true for the r-momentum constraint (15); it vanishes only because of a subtle cancellation of the terms

$$\tfrac{2}{3}\tilde{U}_{,r} + \tilde{U}(-\tfrac{4}{3}P_r + 2r^{-1}) = 0 \tag{45}$$

for the Schwarzschild solution. Each separate term in this equation is large (in particular close to the inner boundary) and the violation of the r-momentum constraint in the perturbed evolutions is dominated by the finite-differencing error of these terms for the Schwarzschild background. Therefore we have divided the r-momentum constraint by the norm of a typical term in (45) (roughly 10^2) in order to give a better idea of the relative size of the constraint violation. The results are shown in figure 2. The violation of the momentum constraints decreases by just over an order of magnitude as the resolution is doubled, reasonably close to the expected convergence factor of $2^4 = 16$.

Of prime interest is the gravitational radiation emitted by the perturbed black hole as measured at $\mathscr{I}^+$. It can be represented by the Bondi news function [9]. This function was defined originally by studying the asymptotic behaviour of the metric in a special coordinate system. This coordinate system will in general not agree with the coordinates used in a numerical evolution. Fortunately, Stewart [41] has developed a method for computing the news in an arbitrary coordinate system, working as we do here in terms of a conformally related metric. We begin by specifying a Newman-Penrose [42] null tetrad $(l, n, m, \bar{m})$ that is adapted to $\mathscr{I}^+$ in the sense that

$$m^\alpha \partial_\alpha \psi = 0. \tag{46}$$

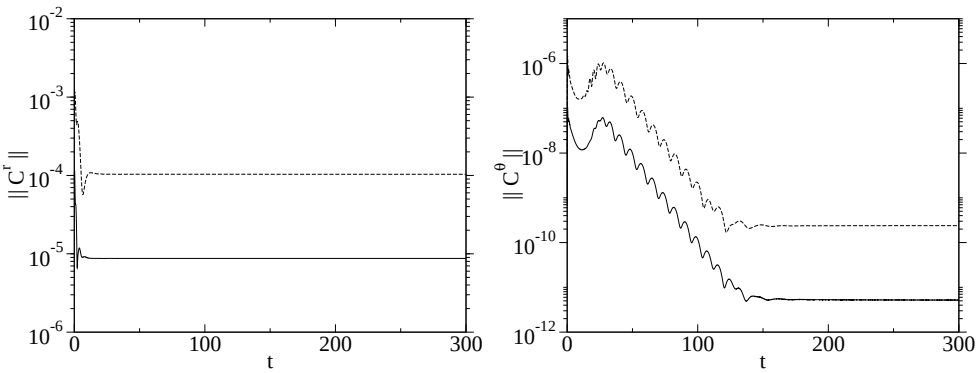

Figure 2. Momentum constraints (15)–(16) as functions of time for two different resolutions $(N_r, N_\theta) = (64, 8)$ (dashed lines) and $(128, 16)$ (solid lines). The r-momentum constraint (left panel) has been normalized by the size of a typical term in (45) as explained in the text.

For definiteness we choose

$$m = \frac{1}{\sqrt{2}r}\left(\mathrm{e}^{-s\eta}\frac{\partial}{\partial\theta} + \mathrm{i}\csc\theta\frac{\partial}{\partial\phi}\right). \tag{47}$$

Apart from the requirement (46) the tetrad is arbitrary. The resulting expressions will be invariant under spin and boost transformations. From the conformal spacetime metric ${}^{(4)}\gamma_{\alpha\beta}$ specified in (3) and (4), we compute the conformal Ricci tensor ${}^{(4)}\tilde{R}_{\alpha\beta}$. The time derivatives in this expression are substituted by using the evolution equations (17)–(21). The Bondi news function is now given by

$$N = \bar{\Phi}_{02} \equiv \bar{m}^\alpha \bar{m}^\beta {}^{(4)}\tilde{R}_{\alpha\beta}. \tag{48}$$

The resulting expression is not yet regular at $\mathscr{I}^+$ but it can be written in a regular form by using the regularity conditions (32), the boundary condition (35) and expressions (B.2) and (B.3) for the radial derivatives of the conformal factor. Ultimately we obtain

$$N \mathrel{\hat{=}} -\mathrm{e}^{-2s\eta}\left[s(\eta_{,rr} + \eta_{,\theta\theta}) - s^2(\eta_{,r})^2 + c\eta_{,\theta} - s^{-1}\eta\right] - \mathrm{e}^{-s\eta}\tilde{\alpha}^{-1}\beta^\theta c\eta_{,r} - \mathrm{e}^{-s\eta}s\tilde{W}_{,r}. \tag{49}$$

The Bondi news function has spin weight -2 and hence we may expand it in spin-weighted spherical harmonics [43] ${}_{-2}Y_{\ell m}$ with $m = 0$ because of the axisymmetry,

$$N(t,\theta)|_{\mathcal{I}^+} = \sum_{\ell=2}^{\infty} N_\ell(t)\ {}_{-2}Y_{\ell 0}(\theta). \tag{50}$$

The $\ell = 2$ contribution is plotted in figure 3. The higher-ℓ contributions are considerably smaller (by at least a factor 10^{-4}) and have not yet converged for the numerical resolutions used here.

After an initial peak when the outgoing part of the wave reaches $\mathscr{I}^+$, we expect the news to consist of a ringing phase due to the quasi-normal mode excitations of the black hole, followed by a polynomial decay ("tail") due to the backscatter of the radiation off the curved background spacetime. These features are apparent in figure 3. However, whereas the ringing phase has converged quite well, the tail is still highly resolution-dependent. Considerably higher resolutions and/or a higher order of accuracy of the discretization will be needed in order to study the tail behaviour.

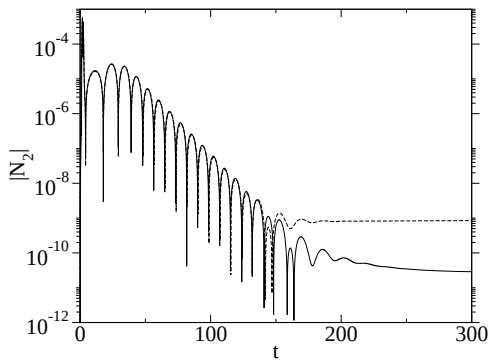

Figure 3. $\ell = 2$ contribution to the Bondi news function (49), evaluated at $\mathscr{I}^+$, as a function of time. Numerical results for two different resolutions are shown, $(N_r, N_\theta) = (64, 8)$ (dashed line) and $(128, 16)$ (solid line).

We expect the quasi-normal mode ringing to have the form

$$N_\ell \propto \mathrm{e}^{-\kappa_\ell t} \sin(\omega_\ell t + \varphi_\ell). \tag{51}$$

The decay rate κ_ℓ and frequency ω_ℓ are estimated by performing a χ^2 fit of (51) to the numerical data for the news at $\mathscr{I}^+$ in the time interval $60 \leqslant t \leqslant 120$. We find $\kappa_2 = 0.0893 \pm 0.0009$ and $\omega_2 = 0.3738 \pm 0.0012$. These values correspond to the high-resolution run and the errors have been estimated by comparing with the low-resolution run. This numerical result is consistent with the linearized-theory result from Leaver's continued-fraction method [44], $\kappa_2 = 0.08896$ and $\omega_2 = 0.37367$.

5. Conclusions

The objective of this paper was to demonstrate that stable numerical evolutions of the Einstein equations on hyperboloidal slices extending to future null infinity $\mathscr{I}^+$ can be obtained. While there has been extensive numerical work [14, 15, 16] using the regular conformal field equations [13] on such foliations, this is, as far as the author is aware, the first result using directly the Einstein equations in a dynamical situation. The advantage of this approach is that it is more similar to formulations of the Einstein equations on (truncated) Cauchy hypersurfaces that have been used successfully in numerical relativity for a long time.

In this paper, we assumed spacetime to be axisymmetric in order to be able to experiment with different ways of treating $\mathscr{I}^+$ numerically in a relatively short computational time. The axisymmetric reduction of the Einstein equations we used (section 2) is similar to previous works [25, 26, 27] but with a constant-mean-curvature slicing condition instead of maximal slicing.

The main new difficulty in adapting a formulation of the Einstein equations on Cauchy slices to hyperboloidal slices is the treatment of the formally singular terms in the evolution equations at $\mathscr{I}^+$. We applied two different methods [23] in order to obtain regular versions of these equations at $\mathscr{I}^+$ (section 2.4). For the evolutions presented in this paper, we used Penrose's [30] result on the vanishing of the conformal Weyl tensor at $\mathscr{I}^+$. For this to hold, certain smoothness assumptions on the conformal metric at $\mathscr{I}^+$ must be satisfied. An alternate method that does not require these assumptions is based on Taylor-expanding the fields near $\mathscr{I}^+$ and

evaluating the singular elliptic equations order by order; with this information, the apparently singular terms in the evolution equations can be evaluated (Appendix B). This alternate form of the evolution equations at $\mathscr{I}^+$ was found to be stable as well and to yield comparable results to within numerical error. Future work should focus on this latter approach as it requires less restrictive smoothness assumptions and is most likely compatible with the so-called polylogarithmic behaviour at $\mathscr{I}^+$ [32].

Our numerical implementation (section 3) uses fairly standard techniques: fourth-order finite differences, the method of lines with a fourth-order Runge-Kutta scheme for the evolution equations, and a multigrid elliptic solver. The only non-standard modification to the multigrid solver is the use of a line relaxation in the radial direction in order to deal with the singular elliptic equations. With this method, no problems with the convergence of multigrid at the singular boundary were encountered. For the evolution equations, the usual Kreiss-Oliger dissipation [33] sufficed to ensure stability; no special smoothing operations at $\mathscr{I}^+$ were required.

We were able to evolve Schwarzschild spacetime for $1000M$ (M being the black hole mass) without any signs of instabilities and with nearly perfect fourth-order convergence (section 4). Next we included a small gravitational perturbation. In order to demonstrate the consistency and convergence of the scheme we monitored the momentum constraints during the evolution. We derived a regular expression for the Bondi news function at $\mathscr{I}^+$ [9, 41] representing the outgoing gravitational radiation. From this we computed the frequency and decay rate of the quasi-normal mode radiation and found good agreement with the tabulated values from linearized theory. The numerical resolutions we were able to reach were not yet high enough in order to study the subsequent polynomial decay (the "tail").

Currently the code is too slow in order to make runs with higher resolutions feasible (the run at the higher resolution in section 4.1 took about two weeks on a single processor). Not much effort has been spent on optimizing the computational efficiency of the code and there is certainly some room for improvement here. It seems likely, however, that a finite-difference method of higher than fourth order or a pseudospectral method will need to be used in order to reach the computational accuracy needed to study tails.

Although our multigrid solver has optimal computational complexity (linear in the number of unknowns) [34, 35], the fact that our formulation contains elliptic equations is a major drawback on the computational speed. This is likely to be even more severe in the case without spacetime symmetries. From this point of view, a hyperbolic formulation such as the one by Zenginoğlu [19] seems advantageous. It would be interesting to see whether the methods of [23] can be applied to that formulation as well so that regular versions of the evolution equations at $\mathscr{I}^+$ are obtained.

In this first study we imposed axisymmetry in order to be able to experiment with different numerical treatments of $\mathscr{I}^+$ more quickly. The next step will be the extension to spacetimes without any symmetries. As far as the numerical stability of $\mathscr{I}^+$ is concerned, we do not expect any new difficulties here because unlike spherical symmetry, axisymmetry already shares with the non-symmetric case what we believe are the key challenges, namely the existence of a dimension tangential to the conformal boundary and the presence of gravitational radiation. It remains to be seen which formulation of the Einstein equations will be more successful for this purpose. We expect the ideas and methods developed in this work to be applicable to a variety of formulations and gauge choices.

Acknowledgment

I am grateful to Vincent Moncrief for numerous fruitful discussions. Helpful interactions with James Bardeen, Luisa Buchman, Harald Pfeiffer, Olivier Sarbach, John Stewart and Anıl Zenginoğlu are much appreciated. I am supported by a Research Fellowship at King's College Cambridge.

Appendix A. Further details on the solution of the elliptic equations

Appendix A.1. Quasi-isotropic gauge conditions

The quasi-isotropic gauge conditions (6) and (7) are formally equivalent to the (inhomogeneous) Cauchy-Riemann equations. In order to solve them, one usually combines derivatives of these equations to obtain two decoupled Poisson equations, which can easily be solved. However, care must be taken so that the solution to the second-order Poisson equations is in fact also a solution to the original first-order Cauchy-Riemann equations (in general the two may differ by integration constants). We use the following approach.

The quasi-isotropic gauge conditions (6) and (7) are

$$0 = \mathcal{S}^r \equiv \beta^r{}_{,r} - \beta^\theta{}_{,\theta} - r^{-1}\beta^r - \tilde{\alpha}\tilde{U}, \tag{A.1}$$

$$0 = \mathcal{S}^\theta \equiv \beta^r{}_{,\theta} + r^2\beta^\theta{}_{,r} - 2\tilde{\alpha}\tilde{K}^r{}_\theta. \tag{A.2}$$

Derivatives of these are combined to obtain a scalar Poisson equation,

$$\begin{aligned} 0 = -\mathcal{S}^r{}_{,\theta} + r^{-2}\mathcal{S}^\theta{}_{,r} = \beta^\theta{}_{,rr} + r^{-1}\beta^\theta{}_{,r} + r^{-2}\beta^\theta{}_{,\theta\theta} - 2r^{-1}\tilde{\alpha}_{,r}\tilde{K}^r{}_\theta + r^{-2}\tilde{\alpha}_{,\theta}\tilde{U} \\ - 2r^{-2}\tilde{\alpha}\tilde{K}^r{}_{\theta,r} + r^{-2}\tilde{\alpha}\tilde{U}_{,\theta} + 2r^{-3}\tilde{\alpha}\tilde{K}^r{}_\theta. \end{aligned} \tag{A.3}$$

This equation is solved for β^θ using multigrid, with homogeneous Dirichlet boundary conditions.

However, we do *not* solve the corresponding Poisson equation for β^r. Instead, we observe that once β^θ is known we can immediately integrate (A.1) and (A.2) to find β^r. First, (A.2) is integrated along the outer boundary $\mathscr{I}^+$ to determine β^r there. The integration constant can be chosen arbitrarily, e.g. by requiring the average of β^r along $\mathscr{I}^+$ to agree with its value for the exact Schwarzschild solution. Next, (A.1) is integrated from each point on the outer boundary towards the interior. In this way we ensure that $\mathcal{S}^r = 0$ everywhere. We have also enforced $\mathcal{S}^\theta \mathrel{\hat{=}} 0$ at the boundary. What remains to be shown is that $\mathcal{S}^\theta = 0$ in the interior. But this follows immediately from (A.3): given that we already have $\mathcal{S}^r = 0$ everywhere, this equation reduces to $\mathcal{S}^\theta{}_{,r} = 0$, and together with the initial condition $\mathcal{S}^\theta \mathrel{\hat{=}} 0$ this implies $\mathcal{S}^\theta = 0$ everywhere.

Apart from ensuring that the first-order conditions (A.1) and (A.2) are indeed satisfied, we also avoid solving another elliptic equation (for β^r) and thus save computational time.

Appendix A.2. Momentum constraints

For the intial data only, the momentum constraints are solved using a method similar to the one due to York [45]. We introduce a vector V^A and write the extrinsic curvature variables as

$$\tilde{U} = \psi^2(V^r{}_{,r} - V^\theta{}_{,\theta} - r^{-1}V^r) \equiv \psi^2 V_-, \tag{A.4}$$

$$\tilde{K}^r{}_\theta = \tfrac{1}{2}\psi^2(V^r{}_{,\theta} + r^2 V^\theta{}_{,r}) \equiv \tfrac{1}{2}\psi^2 V_+, \tag{A.5}$$

$$\tilde{W} = \psi^2 \hat{W}. \tag{A.6}$$

Note the similarity of (A.4) and (A.5) with (6) and (7). The field $\hat{W}$ can be freely specified. The substitutions (A.4)–(A.6) completely decouple the momentum constraints (15) and (16) from the remaining elliptic equations:

$$\begin{aligned} 0 = {} & \tfrac{2}{3}V^r{}_{,rr} + \tfrac{1}{2}r^{-2}V^r{}_{,\theta\theta} - \tfrac{1}{6}V^\theta{}_{,r\theta} - \tfrac{2}{3}V^\theta{}_{,\theta} + \tfrac{1}{3}s\hat{W}_{,r} + r^{-1}s\hat{W} \\ & + V_-(s\eta_{,r} + \tfrac{4}{3}r^{-1}) + r^{-2}V_+(s\eta_{,\theta} + c\eta + \tfrac{1}{2}\tfrac{c}{s}), \end{aligned} \tag{A.7}$$

$$\begin{aligned} 0 = {} & \tfrac{1}{6}V^r{}_{,r\theta} + \tfrac{1}{2}r^2 V^\theta{}_{,rr} + \tfrac{1}{3}V^\theta{}_{,\theta\theta} - \tfrac{2}{3}r^{-1}V^r{}_{,\theta} + \tfrac{1}{3}s\hat{W}_{,\theta} + \tfrac{4}{3}c\hat{W} \\ & - V_-(s\eta_{,\theta} + c\eta) + V_+(s\eta_{,r} + 2r^{-1}). \end{aligned} \tag{A.8}$$

We take V^A to agree with the corresponding vector computed from the exact Schwarzschild solution at the radial boundaries, in particular we have $V^A \mathrel{\hat{=}} 0$ at $\mathscr{I}^+$, and V^θ also vanishes at the inner boundary. The angular parity of V^A is identical with that of β^A (table 1).

Appendix B. Alternate regularized evolution equations

In this appendix we derive alternate regular forms of the evolution equations at $\mathscr{I}^+$ using the Taylor expansion method developed in [23]. Within a hyperboloidal hypersurface t = const, all the fields are expanded in finite Taylor series about $\mathscr{I}^+$ ($r = 1$ in our case),

$$u(x^i) = \sum_{n=0}^{N} \frac{1}{n!} u_n(\theta,\phi)(r-1)^n, \qquad u_n = \lim_{r\nearrow 1} \partial_r^n u. \tag{B.1}$$

These series are substituted in the singular elliptic equations and evaluated order by order. Again we have found a computer algebra programme [31] to be very helpful here. From the Hamiltonian constraint (14) we obtain

$$\psi_{,r} \mathrel{\hat{=}} -\tfrac{1}{3}K\mathrm{e}^{s\eta}, \tag{B.2}$$

$$\psi_{,rr} \mathrel{\hat{=}} -K\mathrm{e}^{s\eta}(\tfrac{1}{2}s\eta_{,r} + \tfrac{1}{3}), \tag{B.3}$$

$$\psi_{,rrr} \mathrel{\hat{=}} K\mathrm{e}^{s\eta}\left\{\tfrac{2c}{3s}(s\eta)_{,\theta} + \tfrac{1}{3}(s\eta)_{,\theta\theta} - \tfrac{1}{3}\left[(s\eta)_{,\theta}\right]^2 + \tfrac{2}{3}s\eta_{,rr} + \tfrac{5}{12}(s\eta_{,r})^2 + \tfrac{2}{3}s\eta_{,r}\right\}. \tag{B.4}$$

The slicing condition (12) yields

$$\tilde{\alpha}_{,r} \mathrel{\hat{=}} \tilde{\alpha}(\tfrac{1}{2}s\eta_{,r} + 1), \tag{B.5}$$

$$\begin{aligned} \alpha_{,rr} \mathrel{\hat{=}} {} & \tilde{\alpha}\left[\tfrac{3c}{2s}(s\eta)_{,\theta} + \tfrac{1}{2}(s\eta)_{,\theta\theta} + \tfrac{1}{2}s\eta_{,rr} - \tfrac{1}{2}(s\eta_{,r})^2 + s\eta_{,r} + 1\right] \\ & + \tfrac{c}{2s}\tilde{\alpha}_{,\theta} + \tfrac{1}{2}\tilde{\alpha}_{,\theta\theta} - \tfrac{3}{2}\tilde{\alpha}_{,\theta}(s\eta)_{,\theta}. \end{aligned} \tag{B.6}$$

From the momentum constraints (15) and (16) we obtain, respectively,

$$s\tilde{W}_{,r} \mathrel{\hat{=}} -2\tilde{U}_{,r} + \tfrac{3}{2}\mathrm{e}^{-s\eta}(s\eta_{,r})^2, \tag{B.7}$$

$$\tilde{K}^r{}_{\theta,r} \mathrel{\hat{=}} \mathrm{e}^{-s\eta}\left[-c\eta_{,r} - \tfrac{1}{2}(s\eta_{,r})_{,\theta} + s\eta_{,r}(s\eta)_{,\theta}\right]. \tag{B.8}$$

Substituting the Taylor expansions (B.1) in the right-hand sides of the evolution equations (19)–(21) and using the above results (B.2)–(B.8) for the radial derivatives of the fields, together with the regularity conditions (32) and the boundary condition

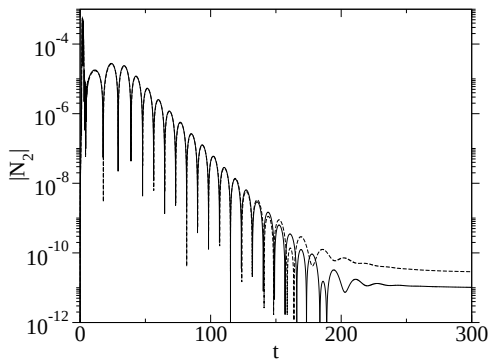

Figure B1. $\ell = 2$ contribution to the Bondi news function (49) at $\mathscr{I}^+$ for an evolution using regularization at $\mathscr{I}^+$ based on Taylor expansions (solid line) as compared with the approach based on Penrose's smoothness assumption (dashed line) that was used in section 4. The numerical resolution is $(N_r, N_\theta) = (128, 16)$.

(35), we obtain the following regular forms of the evolution equations at $\mathscr{I}^+$.

$$\tilde{W}_{,t} \hat{=} \mathrm{e}^{-2s\eta}\big\{\tilde{\alpha}\left[c(s^{-1}\eta)_{,\theta} + \eta_{,\theta\theta} + \eta_{,rr} - s(\eta_{,r})^2 - \eta\right] + \tilde{\alpha}_{,\theta}(\tfrac{c}{s}\eta + \eta_{,\theta}) - (s^{-1}\tilde{\alpha}_{,\theta})_{,\theta}\big\} + \mathrm{e}^{-s\eta}\tilde{\alpha}\tilde{W}_{,r} + \mathrm{e}^{-s\eta}\beta^\theta[\eta_{,r}(c\eta - 2\tfrac{c}{s} + s\eta_{,\theta}) - \eta_{,r\theta}], \quad \text{(B.9)}$$

$$\tilde{K}^r{}_{\theta,t} \hat{=} 0, \quad \text{(B.10)}$$

$$\tilde{U}_{,t} \hat{=} -\tfrac{1}{2}s\tilde{W}_{,t}. \quad \text{(B.11)}$$

Notice in particular how (B.10) and (B.11) are compatible with the regularity conditions (32).

Figure B1 shows the Bondi news function at $\mathscr{I}^+$ for a numerical evolution using the above Taylor-regularized evolution equations at $\mathscr{I}^+$. The result agrees well with the evolution based on the Penrose regularization technique that was discussed in section 2.4 and used for the evolution shown in figure 3. The discrepancy for times $t \gtrsim 150$ can be attributed to numerical error—figure 3 shows that the solution is still highly resolution-dependent at those late times. The corresponding curves in figures 1 and 2 virtually overlap for the two regularization techniques.

Appendix C. Finite-difference operators

In order to compute derivatives with respect to r, we first compute finite-difference approximations to derivatives with respect to the map coordinate x and then apply the chain rule,

$$u_{,r} = \frac{\mathrm{d}x}{\mathrm{d}r}u_{,x}, \qquad u_{,rr} = \left(\frac{\mathrm{d}x}{\mathrm{d}r}\right)^2 u_{,xx} + \frac{\mathrm{d}^2x}{\mathrm{d}r^2}\,u_{,x}. \quad \text{(C.1)}$$

Here $\mathrm{d}x/\mathrm{d}r$ and $\mathrm{d}^2x/\mathrm{d}r^2$ are computed analytically from the given form of the mapping $r(x)$, equation (34).

Fourth-order accurate finite difference operators are used with respect to both x and θ. It suffices to display their one-dimensional forms here. The centred finite difference operators are

$$u_i' \to \tfrac{1}{12h}(u_{i-2} - 8u_{i-1} + 8u_{i+1} - u_{i+2}), \quad \text{(C.2)}$$

$$u_i'' \to \tfrac{1}{12h^2}(-u_{i-2} + 16u_{i-1} - 30u_i + 16u_{i+1} - u_{i+2}), \quad \text{(C.3)}$$

where h denotes the (uniform) grid spacing and the indices refer to the grid points where the quantities are evaluated. The forward differences are

$$u_0' \to \tfrac{1}{12h}(-25u_0 + 48u_1 - 36u_2 + 16u_3 - 3u_4), \tag{C.4}$$
$$u_1' \to \tfrac{1}{12h}(-3u_0 - 10u_1 + 18u_2 - 6u_3 + u_4), \tag{C.5}$$
$$u_0'' \to \tfrac{1}{12h^2}(45u_0 - 154u_1 + 214u_2 - 156u_3 + 61u_4 - 10u_5), \tag{C.6}$$
$$u_1'' \to \tfrac{1}{12h^2}(10u_0 - 15u_1 - 4u_2 + 14u_3 - 6u_4 + u_5), \tag{C.7}$$

and expressions for the backward differences follow by symmetry.

In the x-direction we use centred differences for $2 \leqslant i \leqslant N_r - 2$, forward differences at $i = 0, 1$ and backward differences at $i = N_r, N_r - 1$. In the θ-direction centred differences are used at all interior grid points $1 \leqslant j \leqslant N_\theta$ (note that ghost points are provided at $j = -1, 0$ and $j = N_\theta + 1, N_\theta + 2$).

The expression $(s^{-1}u)_{,\theta}$ is discretized by finite-differencing the function $s^{-1}u$ with respect to θ. No such special differencing is used for $(s^{-1}u_{,\theta})_{,\theta}$, which we simply expand into $s^{-1}u_{,\theta\theta} - s^{-2}cu_{,\theta}$ and then discretize in the standard way. Mixed derivatives $u_{,x\theta}$ are discretized by applying the finite-difference operators with respect to x and θ subsequently in the obvious way.

We use Kreiss-Oliger dissipation [33], whereby the operator

$$\begin{aligned}(Qu)_i &= \left(\tfrac{\epsilon}{64}h^5 D_+^3 D_-^3 u\right)_i \\ &= \tfrac{\epsilon}{64h}(u_{i-3} - 6u_{i-2} + 15u_{i-1} - 20u_i + 15u_{i+1} - 6u_{i+2} + u_{i+3})\end{aligned} \tag{C.8}$$

is applied to each variable u both in the x and the θ direction and the results added to the discretized right-hand side of the evolution equation for u. Here $D_\pm$ denote the first-order forward and backward finite-differencing operators, and a typical choice of the dissipation parameter is $\epsilon = 1/2$. In the x-direction the above dissipation operator is added at grid points $2 \leqslant i \leqslant N_r - 2$ and in the θ-direction at grid points $2 \leqslant j \leqslant N_\theta - 1$. Including $j = 2, N_\theta - 1$ has been found to be essential in order to eliminate an angular instability.

References

[1] Sarbach O 2007 Absorbing boundary conditions for Einstein's field equations *J. Phys.: Conf. Ser.* **91** 012005

[2] Allen E W, Buckmiller E, Burko L M and Price R H 2004 Radiation tails and boundary conditions for black hole evolutions *Phys. Rev. D* **70** 044038

[3] Dafermos M and Rodnianski I 2004 A note on boundary value problems for black hole evolutions (*E-print* `http://www.arxiv.org/abs/gr-qc/0403034`)

[4] Buchman L T and Sarbach O C A 2006 Towards absorbing outer boundaries in general relativity *Class. Quantum Grav.* **23** 6709–6744

[5] Buchman L T and Sarbach O C A 2007 Improved outer boundary conditions for Einstein's field equations *Class. Quantum Grav.* **24** S307–S326

[6] Rinne O, Buchman L T, Scheel M A and Pfeiffer H P 2009 Implementation of higher-order absorbing boundary conditions for the Einstein equations *Class. Quantum Grav.* **26** 075009

[7] Deadman E and Stewart J M 2009 Numerical relativity and asymptotic flatness *Class. Quantum Grav.* **26** 065008

[8] Szabados L B 2009 Quasi-local energy-momentum and angular momentum in general relativity *Living Rev. Relativity* **12**(4)

[9] Bondi H, van der Burg M G J and Metzner A W K 1962 Gravitational waves in general relativity VII. Waves from axi-symmetric isolated systems *Proc. Royal Soc. London A* **269** 21–52

[10] Sachs R K 1962 Gravitational waves in general relativity VIII. Waves in asymptotically flat space-time *Proc. Royal Soc. London A* **270** 103–126

[11] Winicour J 2005 Characteristic evolution and matching *Living Rev. Relativity* **8**(10)

[12] Reisswig C, Bishop N T, Pollney D and Szilágyi B 2009 Unambiguous determination of gravitational waveforms from binary black hole mergers (*E-print* `http://www.arxiv.org/abs/0907.2637`)
[13] Friedrich H 1983 Cauchy problems for the conformal vacuum field equations in general relativity *Commun. Math. Phys.* **91** 445–472
[14] Frauendiener J 2004 Conformal infinity *Living Rev. Relativity* **7**(1)
[15] Husa S 2002 Problems and successes in the numerical approach to the conformal field equations *Lect. Notes Phys.* **604** 239–260
[16] Husa S 2003 Numerical relativity with the conformal field equations *Lect. Notes Phys.* **617** 159–192
[17] Frauendiener J and Hein M 2002 Numerical evolution of axisymmetric, isolated systems in general relativity *Phys. Rev. D* **66** 124004
[18] Bičák J and Schmidt B 1989 Asymptotically flat radiative space-times with boost-rotation symmetry: The general structure *Phys. Rev. D* **40** 1827–1853
[19] Zenginoğlu A 2008 Hyperbolodial evolution with the Einstein equations *Class. Quantum Grav.* **25** 195025
[20] Friedrich H 1985 On the hyperbolicity of Einstein's and other gauge field equations *Commun. Math. Phys.* **100** 525–543
[21] Zenginoğlu A 2007 *A conformal approach to numerical calculations of asymptotically flat spacetimes* PhD thesis Univ. Potsdam (*E-print* `http://www.arxiv.org/abs/0711.0873`)
[22] Arnowitt R, Deser S and Misner C W 1962 The dynamics of general relativity *Gravitation: an introduction to current research* ed Witten L (New York: Wiley) chap 7
[23] Moncrief V and Rinne O 2009 Regularity of the Einstein equations at future null infinity *Class. Quantum Grav.* **26** 125010 (one of the journal's "Highlights of 2008 and 2009")
[24] Buchman L T, Pfeiffer H P and Bardeen J M 2009 Black hole initial data on hyperboloidal slices (*E-print* `http://www.arxiv.org/abs/0907.3163`)
[25] Rinne O 2008 Constrained evolution in axisymmetry and the gravitational collapse of prolate Brill waves *Class. Quantum Grav.* **25** 135009 (one of the journal's "Highlights of 2008 and 2009")
[26] Garfinkle D and Duncan G C 2001 Numerical evolution of Brill waves *Phys. Rev. D* **63** 044011
[27] Choptuik M W, Hirschmann E W, Liebling S L and Pretorius F 2003 An axisymmetric gravitational collapse code *Class. Quantum Grav.* **20** 1857–1878
[28] Rinne O and Stewart J M 2005 A strongly hyperbolic and regular reduction of Einstein's equations for axisymmetric spacetimes *Class. Quantum Grav.* **22** 1143–1166 (one of the journal's "Highlights of 2004 and 2005")
[29] Andersson L and Moncrief V 2003 Elliptic-hyperbolic systems and the Einstein equations *Ann. H. Poincaré* **4** 1–34
[30] Penrose R 1965 Zero rest-mass fields including gravitation: Asymptotic behaviour *Proc. Royal Soc. London A* **284** 159–203
[31] Hearn A C 2004 *REDUCE User's Manual 3.8* RAND Santa Monica, CA
[32] Andersson L, Chruściel P T and Friedrich H 1992 On the regularity of solutions to the Yamabe equation and the existence of smooth hyperboloidal initial data for Einstein's field equations *Commun. Math. Phys.* **149** 587–612
[33] Kreiss H O and Oliger J 1973 Methods for the approximate solution of time dependent problems Global Atmospheric Research Programme (Publication Series No. 10)
[34] Brandt A 1977 Multilevel adaptive solutions to boundary value problems *Math. Comput.* **31** 333–390
[35] Briggs W L amd Henson V E and McCormick S F 2000 *A Multigrid Tutorial* 2nd ed (SIAM)
[36] Press W H, Teukolsky S A, Vetterling W T and Flannery B P 2007 *Numerical Recipes: The Art of Scientific Computing* 3rd ed (Cambridge University Press)
[37] Brill D R, Cavallo J M and Isenberg J A 1890 K-surfaces in the Schwarzschild space-time and the construction of lattice cosmologies *J. Math. Phys.* **21** 2789–2796
[38] Malec E and Ó Murchadha N 2003 Constant mean curvature slices in the extended Schwarzschild solution and the collapse of the lapse *Phys. Rev. D* **68** 124019
[39] Zenginoğlu A, Núñez D and Husa S 2009 Gravitational perturbations of Schwarzschild spacetime at null infinity and the hyperboloidal initial value problem *Class. Quantum Grav.* **26** 035009
[40] Zenginoğlu A 2009 Asymptotics of black hole perturbations *http://www.arxiv.org/abs/0911.2450*
[41] Stewart J M 1989 Numerical relativity III. The Bondi mass revisited *Proc. Royal Soc. London A* **424** 211–222
[42] Newman E T and Penrose R 1962 An approach to gravitational radiation by a method of spin

coefficients *J. Math. Phys.* **3** 566–578

[43] Newman E T and Penrose R 1966 Note on the Bondi-Metzner-Sachs group *J. Math. Phys.* **7** 863–870

[44] Leaver E W 1985 An analytic representation for the quasi-normal modes of Kerr black holes *Proc. Royal Soc. London A* **402** 285–298

[45] York Jr J W 1979 Kinematics and dynamics of general relativity *Sources of gravitational radiation* ed Smarr L L (Cambridge University Press) pp 83–126